A new approach to detect broken rotor bars in induction machines by current spectrum analysis

G. Didier[a], E. Ternisien[b],*, O. Caspary[b], H. Razik[a]

[a]*Groupe de Recherche en Electrotechnique et Electronique de Nancy, GREEN-CNRS UMR-7037, Université Henri Poincaré, Vandoeuvre-les-Nancy Cedex, France*
[b]*Centre de Recherche en Automatique de Nancy, CRAN-CNRS UMR-7039, Université Henri Poincaré, Vandoeuvre-les-Nancy Cedex, France*

Abstract

This paper deals with a new technique to detect broken rotor bars in polyphase induction machines. Like most techniques, we employ the Fourier Transform of the stator current to make detection. But where the other methods use the Fourier Transform modulus, this alternative approach proposes to analyse its phase. As shown by results, the Fourier Transform phase allows to detect one broken rotor bar when the motor operates under a low load but the method robustness decreases for a half-broken rotor bar. So, in order to improve the diagnosis and to permit the detection of incipient broken rotor bar, the analysis is completed with the Hilbert Transform. This transform provides good results and a partially broken rotor bar can be detected when the load torque is equal or greater than 25%. The main advantage of these methods is that the final decision on the rotor cage state is took without the healthy motor reference.
© 2006 Elsevier Ltd. All rights reserved.

Keywords: Phase analysis; Fourier Transform; Hilbert Transform; Broken bar diagnosis; Induction machines

1. Introduction

Nowadays, no one can deny the important role of asynchronous motor in industry applications. It is well-known that a manufacturing process interruption due to a mechanical or electrical problem induces a significant financial loss for the firm. Interruptions can be caused by rotor faults (broken rotor bars or cracked rotor end ring), stator faults (opening of a stator phase or inter-turn short circuits), rotor–stator eccentricity (static and dynamic eccentricity) and bearing failures [1,2]. In order to avoid such problems, these faults have to be detected to prevent a major failure from occurring.

Broken rotor bars rarely cause immediate failures, especially in large multi-pole (slow speed) motor. However, if there are enough broken rotor bars, the motor may not start as it may not be able to develop

---

*Corresponding author.

E-mail addresses: gaetan.didier@green.uhp-nancy.fr (G. Didier), eric.ternisien@iutsd.uhp-nancy.fr (E. Ternisien), olivier.caspary@iutsd.uhp-nancy.fr (O. Caspary), hubert.razik@green.uhp-nancy.fr (H. Razik).

sufficient accelerating torque. Regardless, the presence of broken rotor bars precipitates deterioration in other components that can result in time-consuming and expensive fixes.

Various techniques have been developed to detect broken rotor bars in induction motors. We can quote vibration measurement [3], temperature measurement [4], coils to monitor the motor axial flux [5] or the radial flux [6], Park's Vector current monitoring [7], artificial intelligence-based techniques [8]. However, the most popular techniques are based on the monitoring of the stator current spectrum (called motor current signature analysis) because of its non-intrusive feature [9–12]. In this technique, the amplitudes of the lateral bands created by the rotor fault around the supply frequency are monitored. An augmentation of these amplitudes allows dimensioning the failure's degree. Others use the instantaneous power spectrum of one stator phase to calculate a global fault index [13]. The disadvantage of all these methods is that the knowledge of the healthy motor stator current is necessary to take a decision about the rotor state.

In this paper, a broken rotor bar detection method using the line current discrete Fourier transform (DFT) phase is proposed. This technique does not require the healthy motor current knowledge anymore, which is a major advantage compared to the classical ones. We will show that the basically calculated phase give good results when the motor operates near its nominal load. For weak load, the results obtained are not robust enough for the detection of an incipient rotor fault. This problem will be solved by using the Hilbert Transform (HT) applied to the line current spectrum modulus. Thanks to this method, the diagnosis of a partially broken rotor bar could be carried out without reference even if the motor operates at low load (25% of the rated torque).

2. Current monitoring

Consider an ideal three-phase supply and an asynchronous motor connected in wye. Thus, the instantaneous current circulating in one phase is defined as

$$i_{s0}(t) = \sqrt{2}I_s \sin(\omega_s t - \varphi) \tag{1}$$

with regard to the instantaneous voltage

$$v(t) = \sqrt{2}V_s \sin(\omega_s t). \tag{2}$$

The terms φ, f_s, and ω_s, respectively, represent the phase angle between the voltage and the line current, the fundamental frequency, and the fundamental pulsation $\omega_s = 2\pi f_s$.

When one bar breaks, a rotor asymmetry is created. This asymmetry involves the appearance of a backward rotating field at the slip frequency sf_s (s is the slip of the induction machine in p.u.). The representation of this rotating field in the stator current spectrum is an additional component at frequency $f_{bb_1}^- = (1 - 2s)f_s$. This cyclic current variation causes a speed oscillation at twice the slip frequency $2sf_s$ [14] and finally, this speed oscillation induces, in the stator current spectrum, an upper component at $f_{bb_1}^+ = (1 + 2s)f_s$, and so on. By extension, the broken rotor bar creates additional components in the spectrum modulus at frequencies given by [14]

$$f_{bb_k}^\pm = (1 \pm 2ks)f_s, \quad k = 1, 2, 3, \ldots. \tag{3}$$

The effects of a broken rotor bar can be seen in Fig. 1. Fig. 1(a) represents the line current spectrum in the case of a healthy rotor, and Fig. 1(b) with one broken rotor bar. The presence of a rotor fault increases the amplitude of components situated at frequencies $f_{bb_k}^\pm$. The amplitude of the latter are dependent of three factors. The first is the motor's load inertia, the second is the motor's load torque (current in the rotor bars) and the third is the severity of the rotor fault. For example, the component magnitude will be more important with three broken bars than with a fissured bar. The analysis of Fig. 1(a) shows that the current spectrum contains a component at the frequency $f_{bb_1}^- = (1 - 2s)f_s$. This frequency is created by the natural asymmetry existing in all induction motors and is usually used as reference for the rotor fault diagnosis.

The classical broken bar detection methods usually use the monitoring of the line current Fourier Transform modulus. They are based on the appearance or the increase of the component amplitude at frequencies defined in Eq. (3). Appearance or increase are two terms which imply the comparison with a
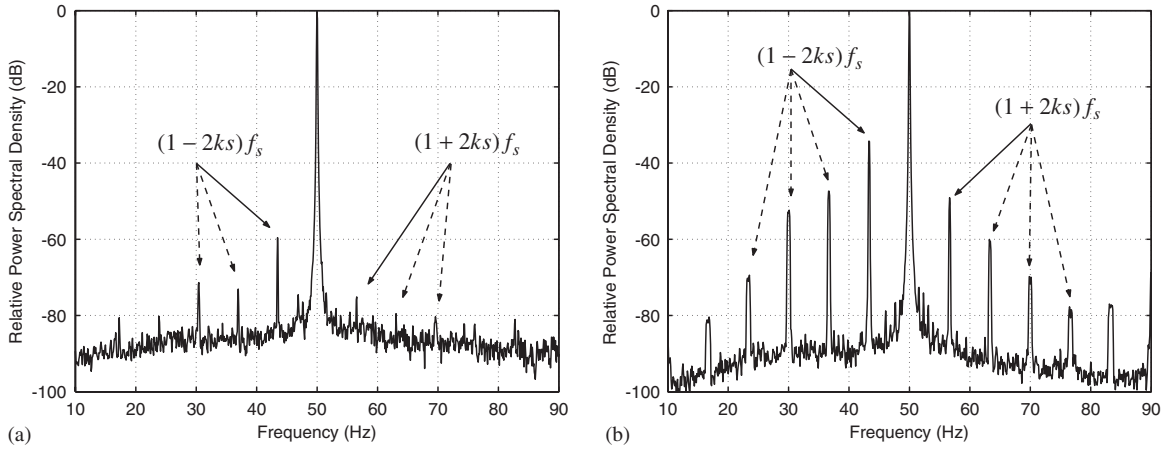
Fig. 1. Line current spectrum modulus for a healthy rotor (a) and a rotor with one broken bar (b).

reference which is often the Fourier Transform modulus of the line current absorbed with a healthy rotor as explained previously.

In this work, the spectrum reference given by the line current of the healthy motor is not necessary anymore. Thus, the detection of broken rotor bars is made without a priori knowledge of the motor state.

3. Discrete Fourier transform (DFT) phase analysis

The DFT is obtained by a discretisation at the sampling frequency of the discrete time Fourier transform (DTFT) given by

$$X(f) = \sum_{n=0}^{N-1} x(n)\mathrm{e}^{-2j\pi n f}, \tag{4}$$

where N is the number of samples of $x(n)$ used to calculate the DTFT. In the case where $x(n) = \mathrm{e}^{2j\pi n f_0}$, the DTFT of $x(n)$ is written as

$$X(f) = \sum_{n=0}^{N-1} \mathrm{e}^{2j\pi n f_0}\mathrm{e}^{-2j\pi n f} = \frac{\sin(N\pi(f-f_0))}{\sin(\pi(f-f_0))}\mathrm{e}^{-j2\pi(N-1)(f-f_0)}, \tag{5}$$

with f_0 the frequency of $x(n)$. In this expression, the Dirichlet function $(\sin(N\pi f)/\sin(\pi f))\,\mathrm{e}^{-j2\pi(N-1)f}$ is introduced by the DTFT of the rectangular window.

Let us consider the following line current expression:

$$i_s(t) = i_{s0}(t) + \sum_{k=1}^{K_l} \frac{\sqrt{2}I_s m_{c_k}^-}{2}\cos(2\pi(f_s - kf_f)t - \varphi_k^-) + \sum_{k=1}^{K_r} \frac{\sqrt{2}I_s m_{c_k}^+}{2}\cos(2\pi(f_s + kf_f)t - \varphi_k^+), \tag{6}$$

where $m_{c_k}^-$ and $m_{c_k}^+$, respectively, represent the modulation index of the left component k and the modulation index of the right component k with regards to the supply frequency f_s in the spectrum modulus. Their values are a function of the fault level in the rotor cage as shown in [13]. Terms φ_k^- and φ_k^+ are the dephasing of the component (left or right) according to the origin (0 rad). Terms K_l and K_r, respectively, represent the number of components at the left and at the right of the carrier frequency present in the line current spectrum for a healthy or faulty rotor. The frequency f_f represents the modulation frequency introduced by the natural asymmetry or by the rotor fault ($f_f = 2sf_s$). The corresponding line current spectra are given in Fig. 1.

Classically, the diagnosis methods use the DFT modulus of the line current defined in Eq. (6) to detect a fault. The DFT phase has been chosen, in this method, because it gives a better representation of the information contained in the line current. Indeed, the components at frequencies $f_{bb_k}^{\pm}$ (Eq. (3)) are present, and their amplitudes are also a function of the fault level, as it is shown in Fig. 2.
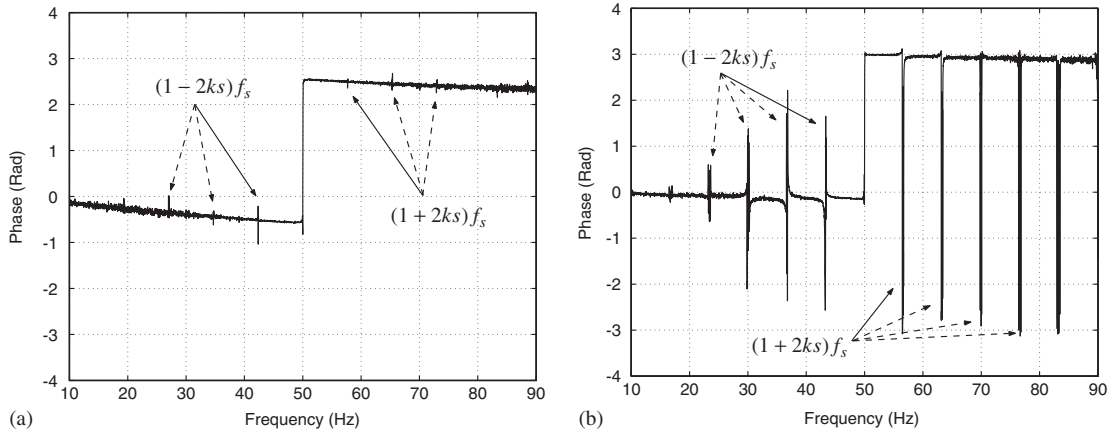
Fig. 2. Line current spectrum phase for a healthy rotor (a) and a rotor with one broken bar (b).

In fact, on each side of the 50 Hz, we notice the presence of phase jumps between $+\pi$ and $-\pi$. These phase jumps are another representation of the components existing in the line current spectrum modulus. Furthermore, in this representation, a phase jump at the 50 Hz frequency is put forward.

The cause of this jump is that the frequencies contained in the line current spectrum are not a multiple integer of the resolution frequency Δf used for the acquisition ($\Delta f = F_e/N$, where F_e represents the sampling frequency).

Indeed, in the case where f_s and f_f are multiple integers of Δf ($f_s = x \Delta f$ and $f_f = x' \Delta f$, where x and x' are integers) the dephasing of all sinusoids contained in the line current expression $i_s(t)$ is obtained (the line current spectrum phase is illustrated in Fig. 3(a) for $f_f = 6$ Hz (parameters used in this case are indexed in Table 1)). However, the case where the frequencies f_s and f_f are not multiple integers of Δf, gives the representation in Fig. 3(b) (by preserving the same parameters). If the modulation indexes increase, which means the appearance of a defect in the rotor cage, jumps present at frequencies $(1 \pm 2ks)f_s$ increase too like in Fig. 3(c) (in this case, parameters used are given in Table 2).

Let us study a simple signal to understand why the phase of the line current spectrum takes this form along the frequency axis. The DTFT of the line current spectrum given at Eq. (6), by taking only into account its fundamental component with $\varphi = 0$ (frequency f_s), can be expressed as

$$
\begin{aligned}
I_s(f) &= \sqrt{2}I_s \sum_{n=0}^{N-1} \sin(2\pi f_s t)\, \mathrm{e}^{-2j\pi nf} \\
&= \sqrt{2}I_s \sum_{n=0}^{N-1} \frac{\mathrm{e}^{j2\pi f_s n} - \mathrm{e}^{-j2\pi f_s n}}{2j}\, \mathrm{e}^{-2j\pi nf} = |I_s(f)|\mathrm{e}^{-\Psi_{I_s}(f)} \\
&= \frac{\sqrt{2}I_s \sin(N\pi(f - f_s))}{2j \sin(\pi(f - f_s))}\, \mathrm{e}^{-j2\pi(N-1)(f-f_s)} \\
&\quad - \frac{\sqrt{2}I_s \sin(N\pi(f + f_s))}{2j \sin(\pi(f + f_s))}\, \mathrm{e}^{-j2\pi(N-1)(f+f_s)}.
\end{aligned}
\tag{7}
$$

In this expression, there are two Dirichlet functions located at frequencies $-f_s$ and $+f_s$. As said previously, the DFT is a sampling of the DTFT. So, when f_s is not a multiple integer of Δf, parasitic undulations are found in the line current spectrum modulus instead of a single component at frequency f_s as shown in Fig. 4(a). Indeed, instead of sampling the DTFT when its values equal 0 (case $f_s = x \Delta f$), the values obtained are the values of the Dirichlet functions.

The same phenomenon occurs for the real and imaginary parts of the spectrum $I_s(f)$. They are not null and depend on values taken by the real and imaginary parts of the DTFT of the line current (Fig. 4(b)).
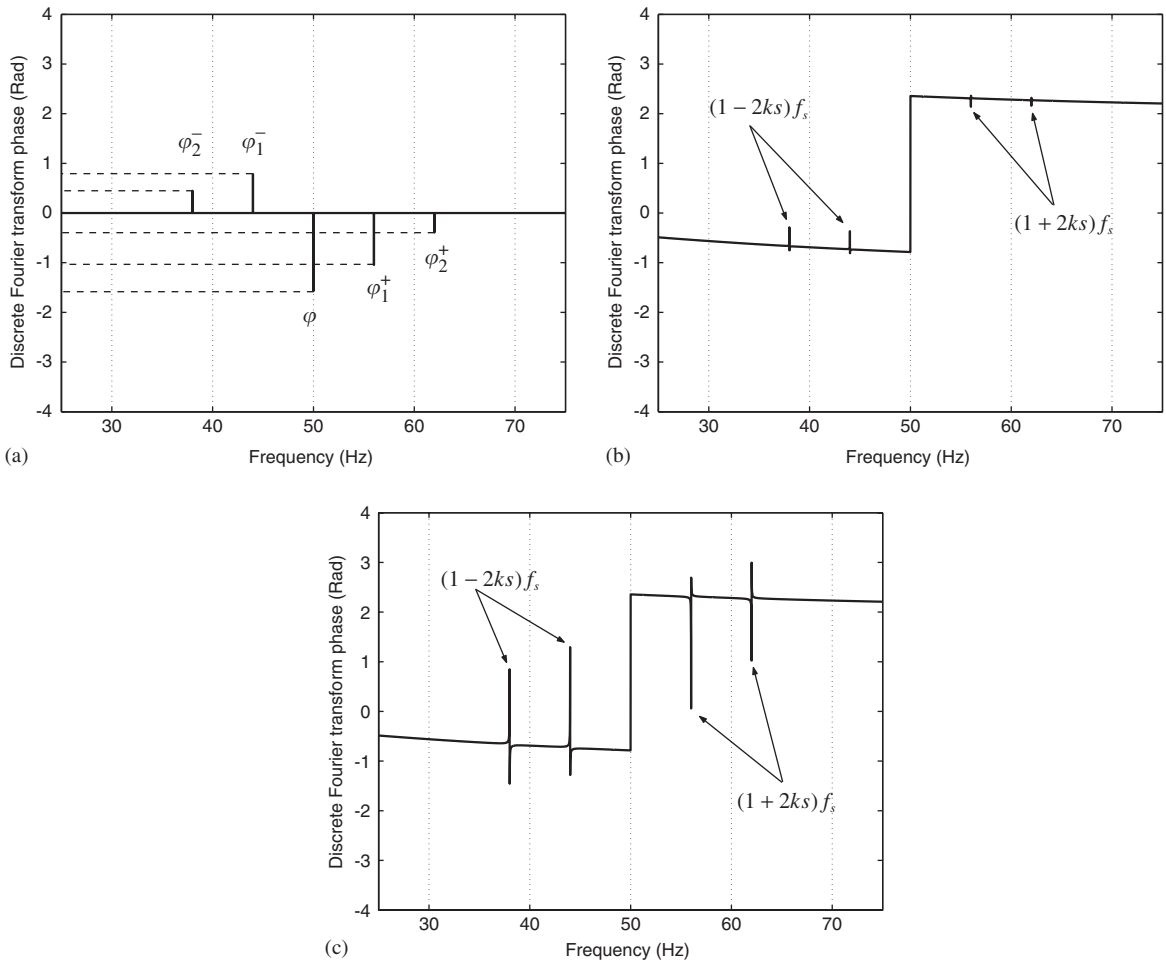
Fig. 3. Current spectrum phase of Eq. (6): (a) and (b) Parameters of Table 1 and (c) parameters of Table 2.

Table 1
Parameters used for Figs. 3(a) and (b) ($K_l = K_r = 2$)

k	1^-	1^+	2^-	2^+
m_{ck}	0.003	0.002	0.0015	0.0005
φ_k	$-\pi/4$	$\pi/4$	$-\pi/7$	$\pi/8$

Table 2
Parameters used for Fig. 3(c) ($K_l = K_r = 2$)

k	1^-	1^+	2^-	2^+
m_{ck}	0.004	0.003	0.002	0.001
φ_k	$-\pi/4$	$\pi/3$	$-\pi/7$	$\pi/8$

As the phase of the DFT $\Psi_{FT}(f)$ varies according to the sign of the real and imaginary parts of $I_s(f)$ (Eq. (8)), we obtain the form given in Fig. 4(c) with a positive jump at the frequency f_s like in Figs. 2(a) and (b). In the ideal case, the result would be a component of value $-\pi/2$ located at the frequency f_s like in
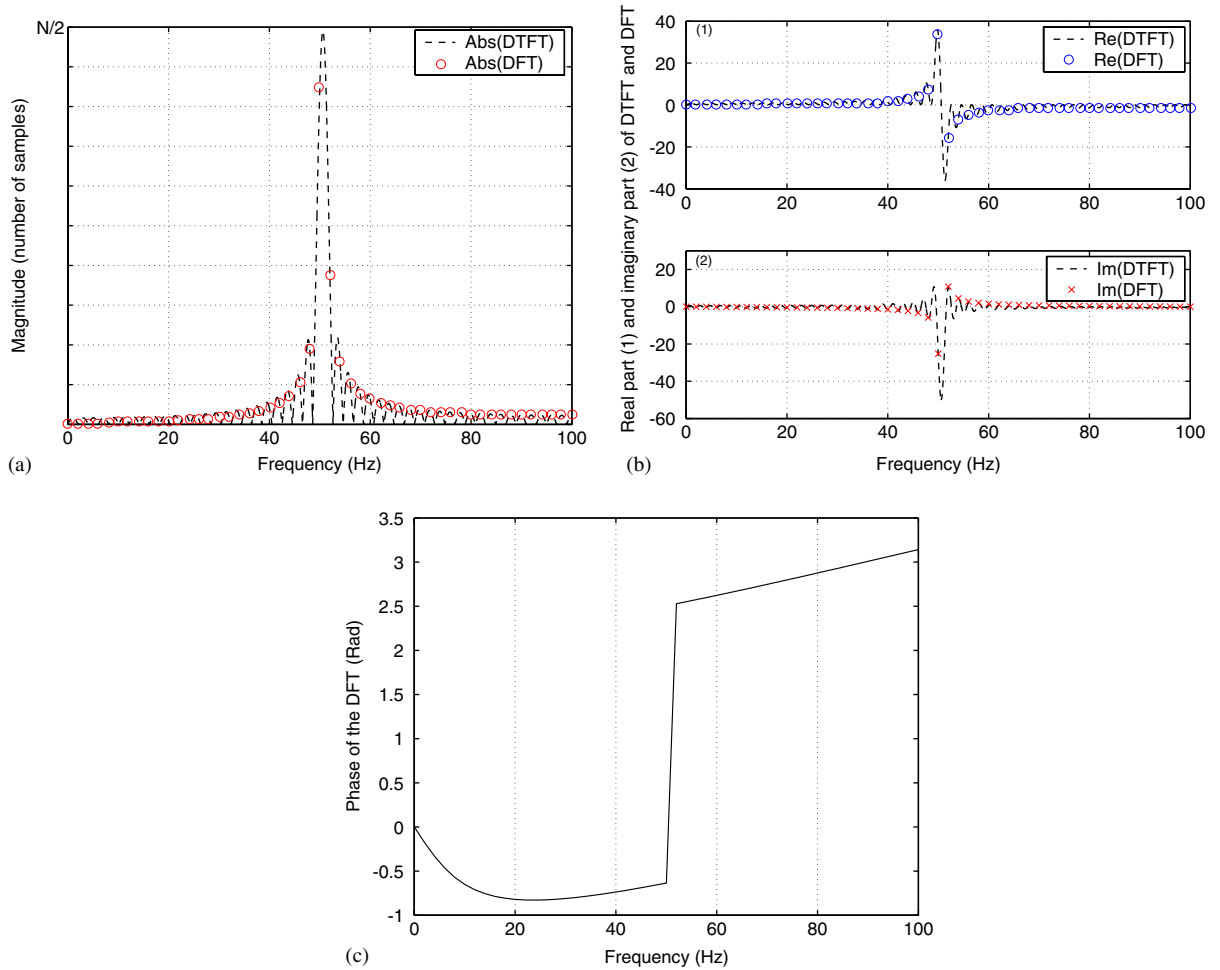
Fig. 4. Discrete Fourier transform of line current (Eq. (7)) with $f_s \neq x\,F_e/N$. (a) modulus of $I_s(f)$; (b) real and imaginary parts of $I_s(f)$; (c) phase of $I_s(f)$.

Fig. 3(a)

$$\Psi_{FT}(f) = \arctan\left(\frac{\mathscr{I}_{FT}(I(f))}{\mathscr{R}_{FT}(I(f))}\right). \tag{8}$$

Nevertheless, the phase jump at 50 Hz is very advantageous for the fault detection because the fundamental component energy problem present in the spectrum modulus is suppressed. This is interesting for the study of high-power motors which have a weak slip (for example, the slip of a 2 MW induction motor is near to 0.3%, which gives a frequency f_f of 0.3 Hz if the fundamental frequency f_s is equal to 50 Hz).

Now, let us consider the particular frequency $(1 - 2s)f_s$. This frequency, in the case of a healthy rotor, corresponds to the natural rotor eccentricity. So, as shown in Fig. 2(a), there is no phase jump at frequency $(1 + 2s)f_s$ because there is no broken rotor bar (in fact a component exists but masked by the noise). That is checked for all load levels studied. On the opposite, when the rotor cage contains a broken bar (Fig. 2(b)), the phase jump at frequency $(1 + 2s)f_s$ is present (like the other components at frequencies given by Eq. (3)).

A simple criterion can be deduced from this observation:

- if there is no phase jump at the frequency $(1 + 2s)f_s$, there is *no default*;
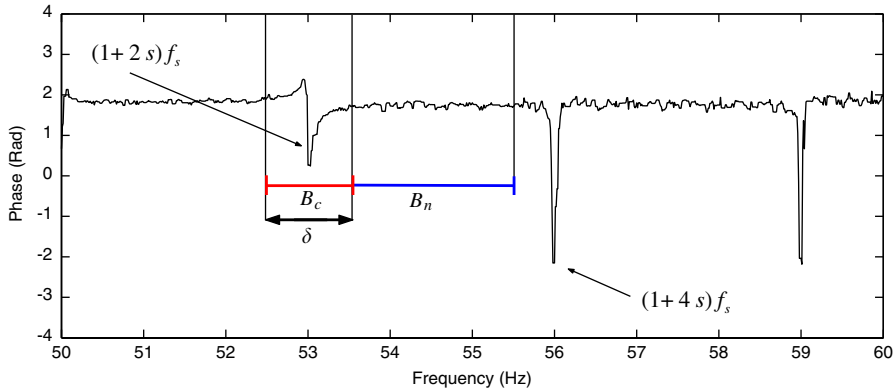- if there is a phase jump at the frequency $(1 + 2s)f_s$, there is *default*.

Fig. 5. Variance calculus intervals on the line current spectrum phase in the frequency band [50–60] Hz.

In order to make a more robust detection and to limit the detection of false alarms, a threshold α has been introduced in the criterion. This threshold compares the variance σ_c of $\Psi_{FT}(f)$ in the interval $B_c = [(1+2s)f_s - \delta/2, (1+2s)f_s + \delta/2]$ where the fault component is located, with the variance σ_n of $\Psi_{FT}(f)$ in the interval $B_n = [(1+2s)f_s + \delta/2, (1+4s)f_s - \delta/2]$ which contains noise. The term δ represents the frequency bandwidth used for the calculus of σ_c (Fig. 5). So the criterion can be reformulated as:

$$\begin{cases} \text{if } \dfrac{\sigma_c}{\sigma_n} > \alpha \;\Rightarrow\; \text{Default,} \\[2mm] \text{if } \dfrac{\sigma_c}{\sigma_n} \leqslant \alpha \;\Rightarrow\; \text{No Default.} \end{cases} \tag{9}$$

Since the detection is based on the appearance of a significant phase jump at frequency $(1+2s)f_s$, the first step of the algorithm is to estimate the slip of the induction motor. The best way to estimate the slip is to use the component at frequency $(1-2s)f_s$ because, in the case of a healthy rotor, only this component is detectable. Moreover, the detection is easier at the left of the 50 Hz due to the greatest amplitude of components. Therefore, the proposed algorithm for the broken bars detection is:

(1) Detection of the maxima (or minima, it depends on the phase shape) at the left of the 50 Hz;
(2) Selection of the 50 Hz nearest maximum ($(1-2s)f_s$ component);
(3) Computation of σ_c and σ_n with respect to the $(1+2s)f_s$ component;
(4) Decision.

In fact, the frequency band used for the maxima research can be limited to the interval $[F_0, 50]$ Hz. The frequency F_0 depends on the maximum slip of the induction motor (at full load). For our motor, the rotation speed at full load is $\Omega = 2804$ rpm, so $s = 6.53\%$ and $2sf_s = 6.53$ Hz. Consequently, F_0 was took equal to 40 Hz.

To help the maxima (or minima) detection, a median filter is used. This filter has a smoother effect and suppress the little peaks in the signal. The results of this method are presented in Section 5.

To ensure the robustness of the previous method, and to detect more precisely the incipient rotor faults, another approach to improve the broken rotor bar diagnosis is proposed.

4. Hilbert Transform (HT) phase analysis

As explained in the previous section, the DFT phase, although the method gives good results, has two disadvantages. The first is the important noise level which makes the maxima detection and the peaks discrimination at the right of the 50 Hz (at low load) difficult. The second is that the shape of the phase is not fixed (see Figs. 8 and 10). Indeed, when studied frequencies are different from Δf, the real and imaginary parts

can take random values. In order to stabilise the phase shape, a solution to control the real and imaginary part values of the DFT spectrum must be found. The idea is to obtain a phase always equal to $-\pi/2$ at the left of f_s and equal to $\pi/2$ at the right of f_s, with no variation excepted at the broken bar frequencies. Consequently, the real part must be null excepted at frequencies $f_{bb_k}^{\pm}$ and f_s.

The solution is to interpret the DFT modulus as the real part of a new signal called "analytic signal". Indeed, as shown in Fig. 6(a), the modulus contains very weak values and dirac impulsions at studied frequencies. So, the shape of the real part is well-known at each frequency point and the signal noise ratio (SNR) is increased.

The analytic signal is obtained by a HT of the line current spectrum modulus. Let us consider a time signal $s(t)$, the analytic signal $\tilde{s}(t)$ can be expressed as

$$\tilde{s}(t) = s(t) + j\rho(t), \tag{10}$$

where

$$\rho(t) = \mathscr{H}(s(t)) = s(t) * \frac{1}{\pi t}. \tag{11}$$

The HT $\mathscr{H}(s(t))$ is defined as the convolution product of the signal $s(t)$ (which becomes the real part of $\tilde{s}(t)$) by a filter whose the impulse response is $h(t) = 1/\pi t$. The analytic signal $\tilde{s}(t)$ is calculated by using different methods [15]. One of these methods is the use of the Fourier Transform. Indeed, the Fourier Transform of the signal $\rho(t)$, which represents the HT of the signal $s(t)$, is given by the following equation:

$$\rho(t) \xrightarrow{\mathscr{F}} -j sgn(f)S(f), \tag{12}$$

where the function $sgn(f)$ and $S(f)$ represent, respectively, the signum function (distribution) given by Eq. (13) and the Fourier Transform of $s(t)$

$$sgn(f) = \begin{cases} +1 & \text{for } f > 0, \\ 0 & \text{for } f = 0, \\ -1 & \text{for } f < 0. \end{cases} \tag{13}$$

Consequently, the analytic signal $\tilde{s}(t)$ can be obtained by using the Fourier Transform with the expression

$$\tilde{s}(t) \xrightarrow{\mathscr{F}} S(f) + j[-j sgn(f)]S(f) = [1 + sgn(f)]S(f) = x(f)S(f), \tag{14}$$

with

$$x(f) = [1 + sgn(f)] = \begin{cases} 2 & \text{for } f > 0, \\ 1 & \text{for } f = 0, \\ 0 & \text{for } f < 0. \end{cases} \tag{15}$$

The Fourier image of the analytic signal is doubled at positive frequencies and cancelled at negative frequencies with respect to $S(f)$. The advantage of this transformation is that the result remains in the same domain as the signal analysed (time for example). The particularity of this paper is that the HT is not applied on the time signal $i_s(t)$ but on its spectrum modulus $|I_s(f)|$. Hence, the analytic signal of this modulus provides:

$$\tilde{I}_s(f) = |I_s(f)| + j I_{HT}(f), \tag{16}$$

with

$$I_{HT}(f) = \mathscr{H}(|I_s(f)|). \tag{17}$$

Eq. (18) represents the diagram used to obtain the analytic signal $\widetilde{I}_s(f)$ with the Fourier Transform

$$
\begin{array}{ccc}
|I_s(f)| & \xrightarrow{\;\mathcal{F}\;} & S(z) \\[4pt]
\Big\uparrow {\scriptstyle \mathcal{R}(\widetilde{I}_s(f))} & & \Big\downarrow {\scriptstyle .\,x(z)} \\[4pt]
\widetilde{I}_s(f) & \xleftarrow{\;\mathcal{F}^{-1}\;} & x(z)S(z) \\[4pt]
\Big\downarrow {\scriptstyle \mathcal{I}(\widetilde{I}_s(f))} & & \\[4pt]
I_{HT}(f) & &
\end{array}
\tag{18}
$$

In this equation z represents the inverse time. The analytic signal phase $\Psi_{HT}(f)$ can be calculated with the expression:

$$
\Psi_{HT}(f) = \arctan\left(\frac{\mathscr{I}(\widetilde{I}_s(f))}{\mathscr{R}(\widetilde{I}_s(f))}\right) = \arctan\left(\frac{I_{HT}(f)}{|I_s(f)|}\right).
\tag{19}
$$

The real part $|I_s(f)|$, the imaginary part $I_{HT}(f)$ and the phase $\Psi_{HT}(f)$ of the analytic signal are shown in Fig. 6 in case of one broken rotor bar.
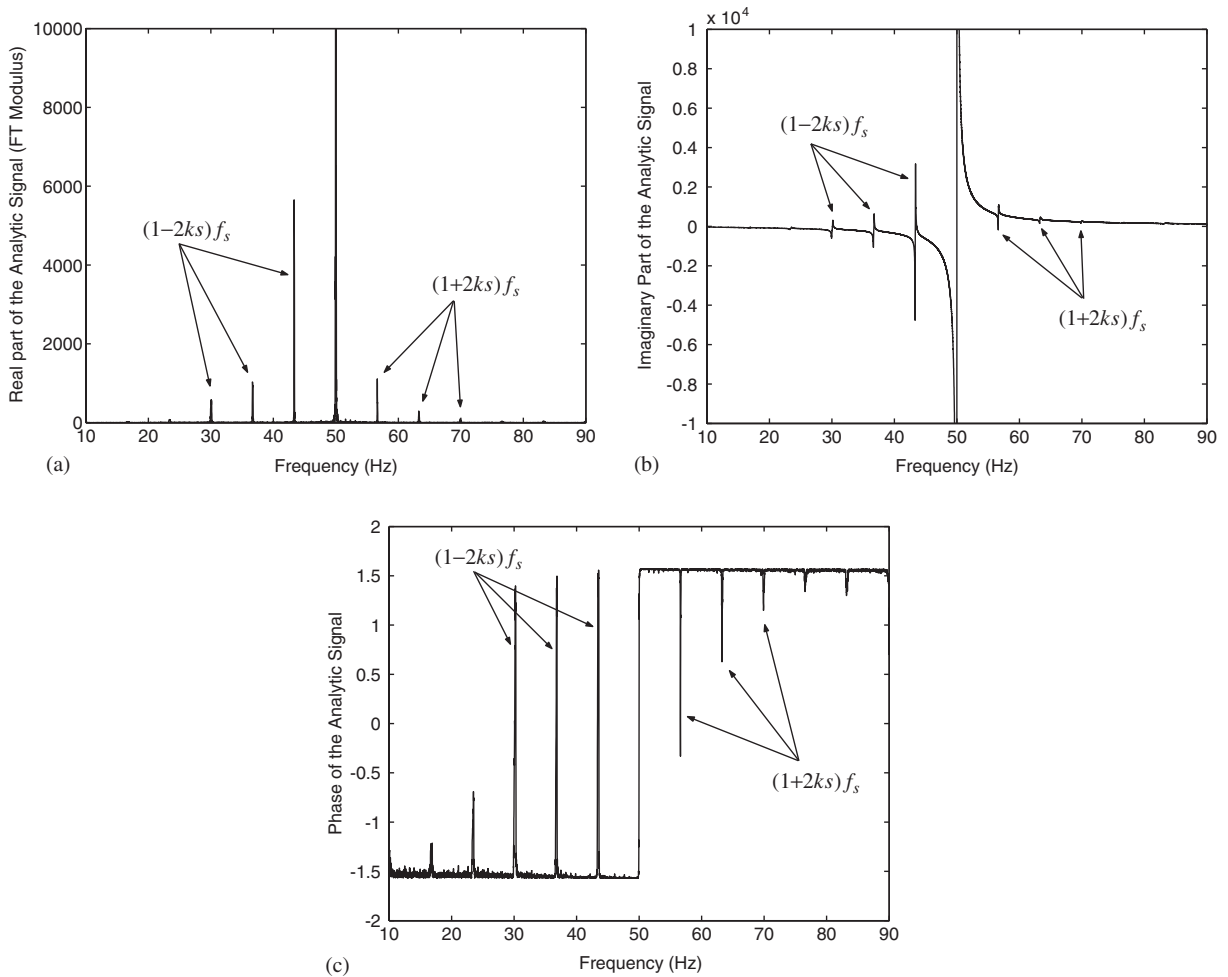

Fig. 6. Real part (a), imaginary part (b) and phase (c) of the analytic signal $\check{I}_s(t)$ (for one broken rotor bar).

In conclusion, the HT applied to the spectrum modulus gives a phase restricted to the interval $[-\pi/2, \pi/2]$. Moreover, the knowledge of the imaginary part from Eq. (11) allows to predict the exact form of the analytic signal phase.

Thanks to the noise reduction, phase jumps are more pronounced which permits an easier detection. The noise level is lower than in $\Psi_{FT}(f)$ because of the redefinition of $|I_s(f)|$ and $I_{HT}(f)$ thanks to the HT. The algorithm remains the same as for the DFT phase detection.

5. Experimental results

The test-bed used in the experimental investigation is composed of one three-phase induction motor of which the specifications are:

- manufacturer: SEW USOCOME
- rated voltage: 380 V
- rated current: 5.9 A
- nominal speed: 2800 rpm
- number of pole: 2
- frequency: 50 Hz
- power: 3 KW

In order to test the effectiveness of the suggested methods, several identical rotors can be exchanged without affecting the electrical and magnetic features, but the noise level can be slightly different especially with a weak load (Fig. 10 with regards to Figs. 10(b) and (c)). The squirrel cage has 28 rotor bars (Fig. 7). The voltage and the line current measurements were made at the nominal rate by an acquisition card with six channels which the sampling frequency is contained in the interval [1 kHz, 1 MHz]. For those two variables, the sampling frequency F_e was 2 kHz and each data length was equal to 2^{18} values. The diagnostic program has been developed on a Matlab platform. The study concerns the case of a partially broken rotor bar (approximately 50% of the bar is bored) and one broken rotor bar. Indeed, the detection of an incipient rotor fault remains, nowadays, still difficult.

The results obtained using the DFT phase are given in Table 3 (for example the notations H-L100 represent a healthy rotor with 100% load and 05b-L25 a partially broken rotor bar with 25% load). Figs. 8 and 10 represent the DFT phase when the torque applied to the machine is equal to 100% and 25% of the rated torque.

The α coefficient was chosen equal to 3. This value was selected according to the experimental results carried out. The results analysis shows us that the detection of one broken rotor bar is possible at a load torque higher than 25%. On the other hand, the detection of an incipient rotor defect (a partially broken rotor bar) can be made only if the load torque applied to the machine is at least equal to 50%.

This non-detection is mainly due to the important noise level in the phase signal. Indeed, noise increases when the load applied to the machine decreases (Figs. 10(a)–(c) in comparison with Figs. 8(a)–(c)). For these operating modes, the variance σ_n is important, which makes the detection of the rotor defect more difficult because the ratio σ_c/σ_n is too weak. So the algorithm of decision considers that the rotor cage presents no defect.

When the asynchronous machine operates with no load, the algorithm of detection does not take any decision. This means that the jump located at the frequency $(1 - 2s)f_s$ is not detectable due to its low amplitude. The current which crosses the rotor bars is not important enough to create a consequent jump at this frequency. Thus, the algorithm cannot evaluate the slip of the asynchronous machine and so the two frequency bands B_c and B_n.

If we consider that an asynchronous machine operates most of its time at its rated torque, the results given by the analyses of the DFT phase are satisfying.

Table 4 shows the results obtained with the analytical signal phase. For these analysis, α was equal to 10. This value is different for the two methods because the SNR of the HT phase is greater than the DFT phase one.
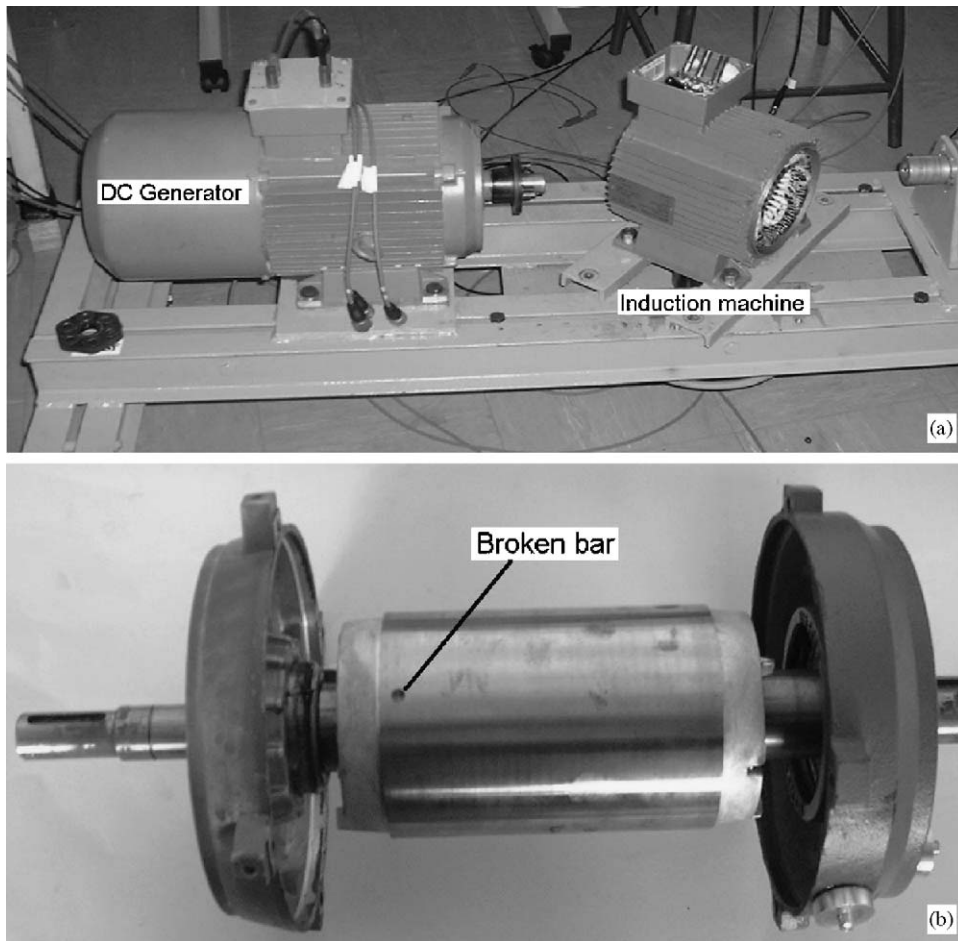
Fig. 7. Test-bed and rotor with one broken bar.

Table 3
Fault detection by DFT phase analysis

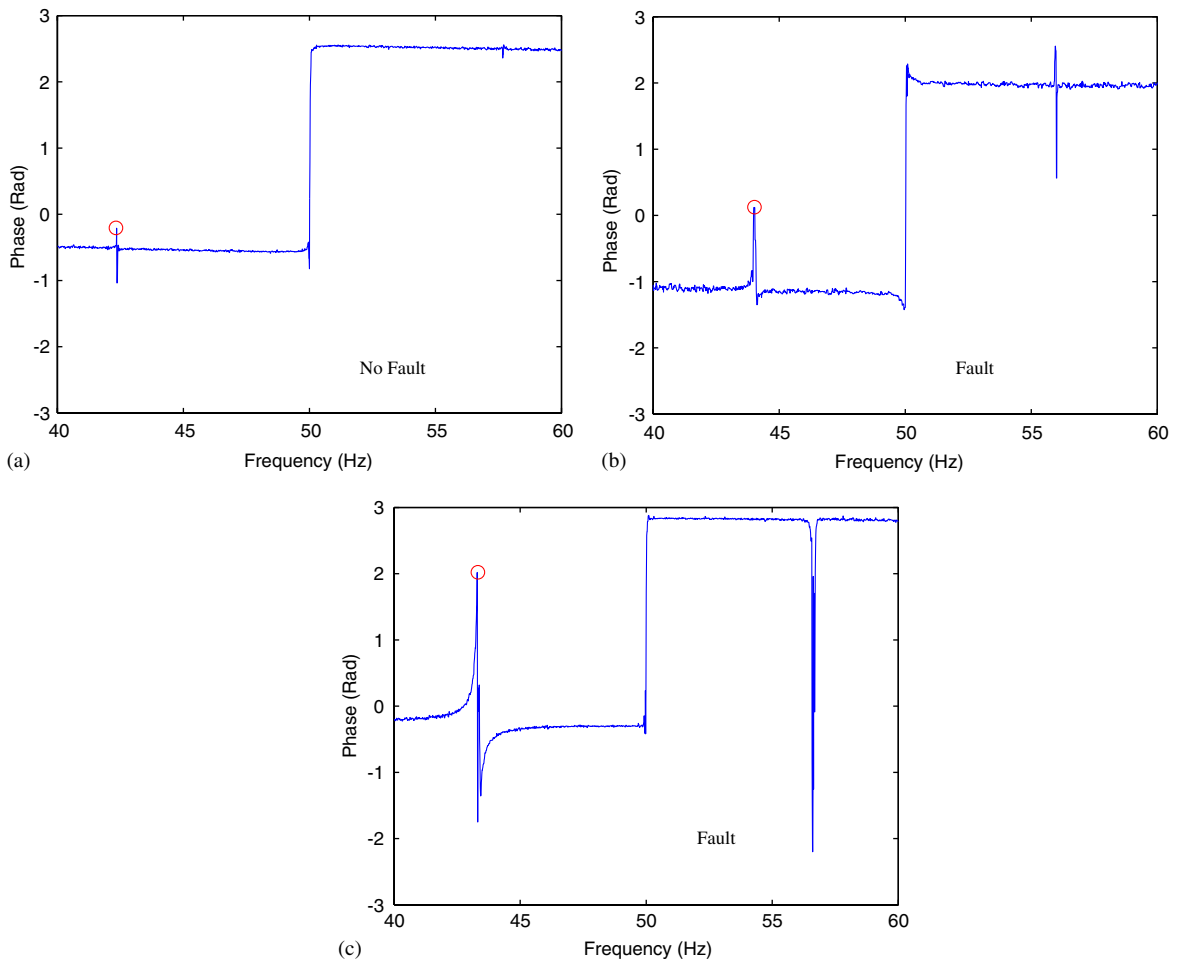| Rotor state	$(1-2s)f_s$ frequency	σ_c	σ_n	$\dfrac{\sigma_c}{\sigma_n}$	No default	Default
H-L100	43.49	0.0037	0.0067	0.5525	X	
05b-L100	44.03	0.0147	0.0008	19.4797		X
1b-L100	43.28	2.6171	0.0002	14500		X
H-L75	45.08	0.0033	0.0034	0.9743	X	
05b-L75	45.74	0.3637	0.0001	2500		X
1b-L75	45.45	0.1827	0.0049	37.4356		X
H-L50	No max detection					No decision
05b-L50	47.13	0.0004	0.0002	2.6286	X	
1b-L50	46.97	0.2113	0.0030	70.4681		X
H-L25	48.42	0.0712	0.0574	1.2412	X	
05b-L25	48.57	0.0004	0.0003	1.1345	X	
1b-L25	48.45	0.0043	0.0006	7.1024		X
H-L0	No max detection					No decision
05b-L0	No max detection					No decision
1b-L0	No max detection					No decision

Fig. 8. Fault detection with the line current spectrum phase analysis under 100% load: (a) healthy rotor; (b) half-broken rotor bar; (c) one broken bar.

Table 4
Fault detection by analytic signal phase analysis

Rotor state	$(1-2s)f_s$ frequency	σ_c	σ_n	$\dfrac{\sigma_c}{\sigma_n}$	No default	Default
H-L100	43.45	0.0003	5.31E−05	5.3785	X	
05b-L100	44.00	0.0038	4.49E−05	84.0466		X
1b-L100	43.54	0.1103	2.51E−05	4390		X
H-L75	45.08	0.0003	5.13E−05	6.2159	X	
05b-L75	45.70	0.0028	5.04E−05	54.6524		X
1b-L75	45.45	0.1103	3.56E−05	3100		X
H-L50	46.79	0.0004	8.86E−05	4.4387	X	
05b-L50	47.14	0.0014	3.66E−05	38.1296		X
1b-L50	47.01	0.0748	12.9E−05	578.6473		X
H-L25	48.40	0.0002	36.9E−05	0.6299	X	
05b-L25	48.56	0.0005	3.50E−05	14.2723		X
1b-L25	48.50	0.0239	35.7E−05	66.966		X
H-L0	No max detection				No decision	
05b-L0	No max detection				No decision	
1b-L0	No max detection				No decision	

With the HT, the two rotor defects (a broken bar and a partially broken bar) are detected when the load torque is contained between 25% and 100% of the rated torque. The non-detection of the jump at frequency $(1 - 2s)f_s$ is always present when the machine is unloaded.

Except this particular case, the results obtained are better compared to those given in Table 3. This better detection is possible because the noise contained in the analytical signal phase is far less important when the machine operates under low-load torque. Figs. 11(a)–(c) illustrate the use of HT applied to the line current spectrum modulus compared to Figs. 10(a)–(c). The weak noise contained in the frequency band $[(1 + 2s) f_s + \delta/2, (1 + 4s)f_s - \delta/2]$ gives a more sensitive detection algorithm in case of incipient rotor defect. Indeed, in this case, the calculation of variances σ_c and σ_n is more optimal than in the previous method. Furthermore, it is obvious that the maxima are more easily detectable (Figs. 9–11).

The key point is that both techniques work with any knowledge of healthy rotor. But for an acceptable response, the load must be at least 25% in order to have a minimum current in the rotor to make the phase jump at $(1 - 2s)f_s$ distingable.

In case of limited number of samples (for example 4096 samples), the broken rotor bar can still be detected by the analytic signal phase method. By contrast, the DFT method provides bad results since the fault is not detected. This is due to the deficient resolution induced by the reduction of the sample number. The HT method is insensitive to this variation thanks to its principle, but a reduction of phase jump amplitude is visible. Consequently, a minimal number of samples is required to make a good detection. For example, in our
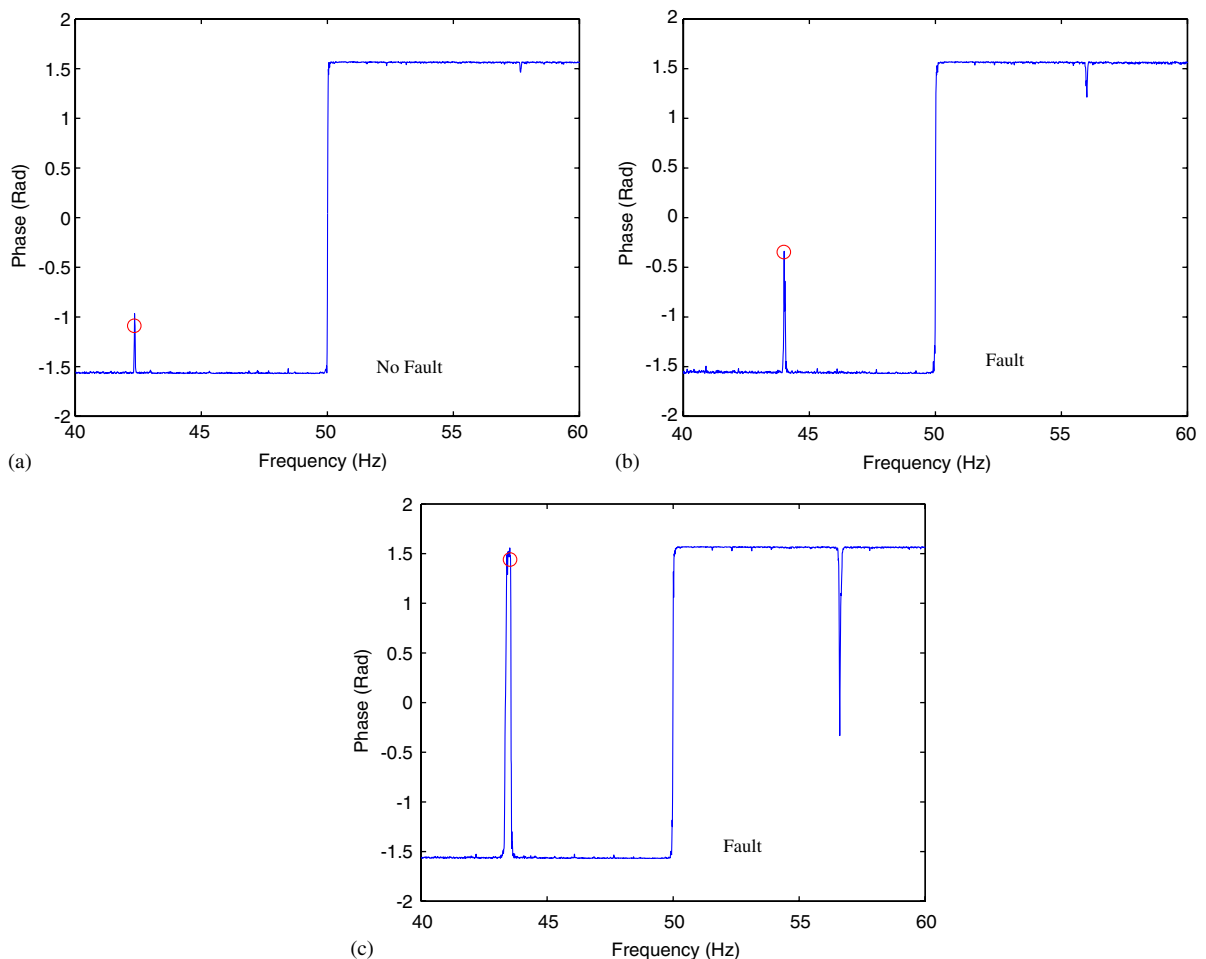

Fig. 9. Fault detection with the analytic signal phase analysis under 100% load: (a) healthy rotor; (b) half-broken rotor bar; (c) one broken bar.
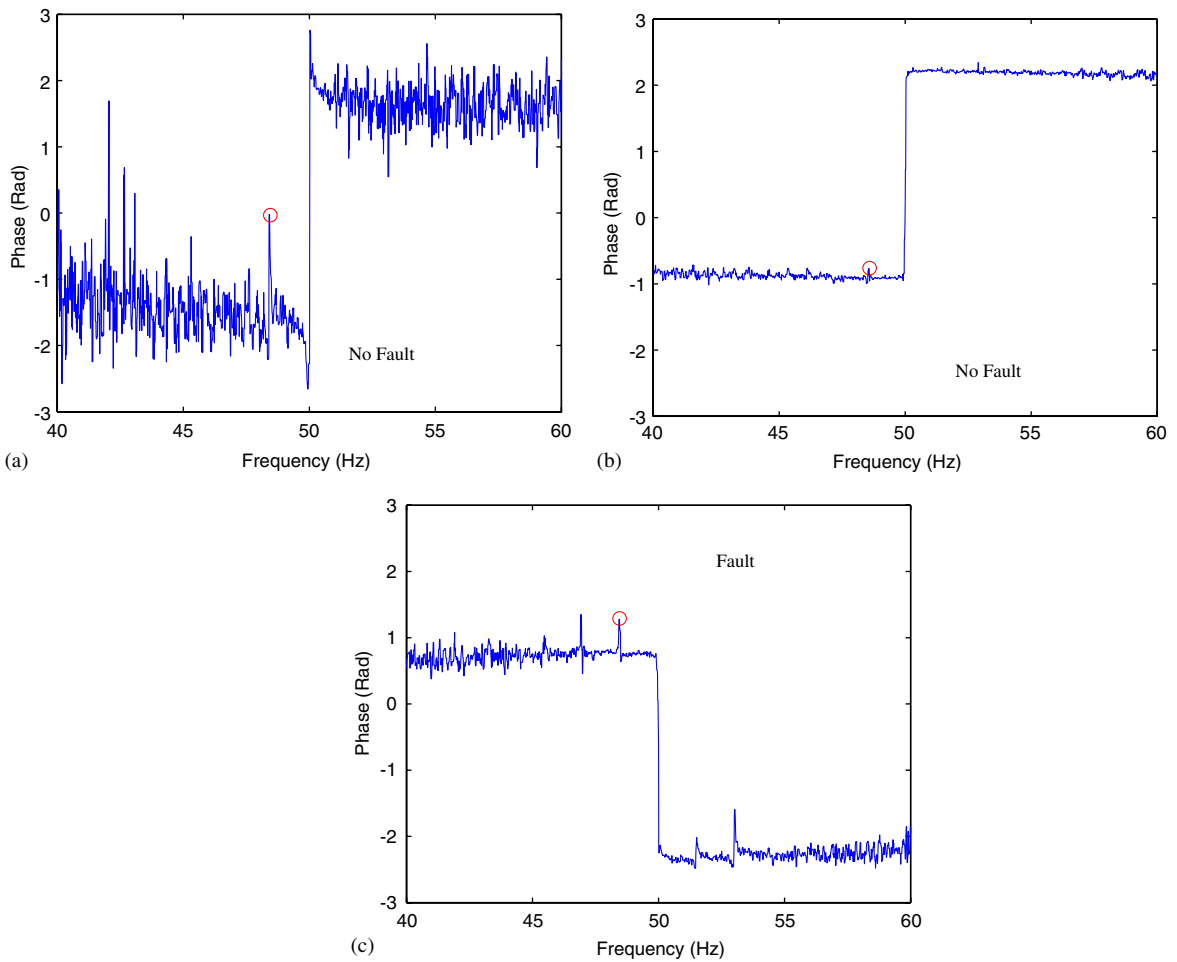
Fig. 10. Fault detection with the line current spectrum phase analysis under 25% load: (a) healthy rotor; (b) half-broken rotor bar; (c) one broken bar.

case, the detection of one broken rotor bar for a full load operation is possible with 4096 samples, but at 50% load, 8192 samples are needed to make rotor fault detection.

6. Conclusion

The proposed methods in this article are based on the analysis of the line current spectrum. We showed that information contained in the spectrum modulus (components at frequencies $(1 \pm 2ks)f_s$) is also visible in the DFT phase at the same frequencies, in the form of phase jumps. Indeed, these phase jumps also depend on the presence or the absence of broken bars in the rotor cage. The results obtained with the DFT phase are satisfying in case of one broken rotor bar, but the importance of the noise level prevents the detection of a partially broken rotor bar. In order to reduce the noise in the phase signal and to make the detection more reliable, a second method is put forward. This one uses the modulus of the line current DFT as the real part of a new complex signal obtained by the HT. This method provides better results since we detect a partially broken rotor bar for a load level superior to 25%. Besides, the HT method is less sensible to number of samples variation than the DFT. This property could make easier the implantation on a digital signal processor (DSP).

The essential point described in this article is the detection without a priori knowledge of the healthy motor. It is distinguished from the traditional methods which need this reference.
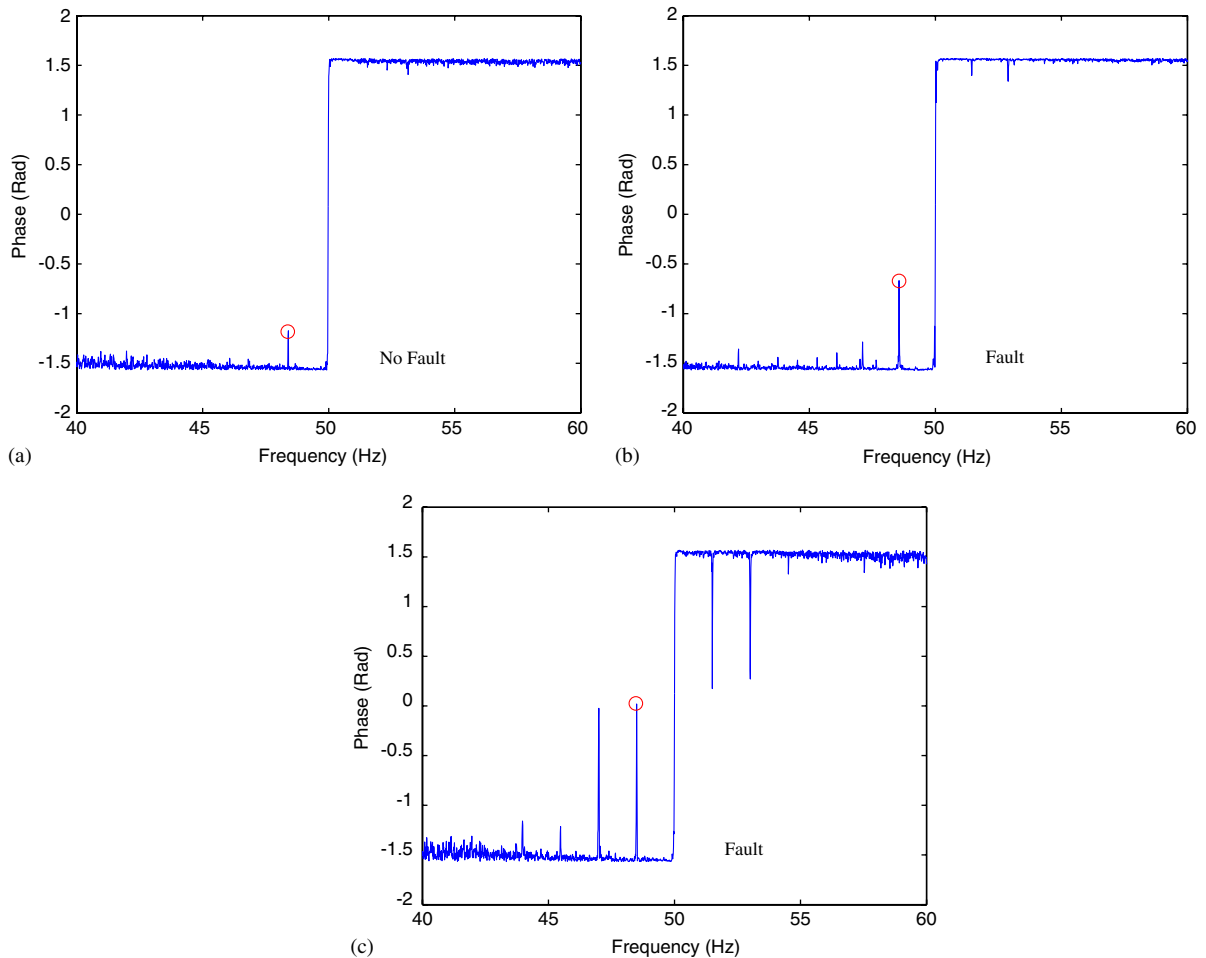
Fig. 11. Fault detection with the analytic signal phase analysis under 25% load: (a) healthy rotor; (b) half-broken rotor bar; (c) one broken bar.

Acknowledgment

References

[1] A.H. Bonnet, Analysis of rotor failures in squirrel cage induction machines, IEEE Transactions on Industry Applications 24 (6) (1988) 1124–1130.

[2] A.H. Bonnet, G.C. Soukup, Cause and analysis of stator and rotor failures in three-phase squirrel-cage induction motors, IEEE Transactions on Industry Applications 28 (4) (1992) 921–937.

[3] S. Pöyhönen, P. Jover, H. Hyötyniemi, Independent component analysis of vibrations for fault diagnosis of an induction motor, Proceedings of the IASTED International Conference Circuits, Signals and Systems, vol. 1, Mexico, May 2003, pp. 203–208.

[4] H. Yahoui, G. Grellet, Measurement of physical signals in the rotating part of an electrical machine by means of optical fibre transmission, Measurement 20 (3) (1997) 143–148.

[5] G.B. Kliman, R.A. Koegl, S. Stein, R.D. Endicott, M.W. Madden, Noninvasive detection of broken rotor bars in operating induction motors, IEEE Transactions on Energy Conversion EC-3 (4) (1988) 873–879.

[6] R. Romary, R. Corton, D. Thailly, J.F. Brudny, Induction machine fault diagnosis using an external radial flux sensor, European Physical Journal—Applied Physics (2005).

[7] M.E.H. Benbouzid, A review of induction motors signature analysis as a medium for faults detection, IEEE Transactions on Industrial Electronics 47 (5) (2000) 984–993.

[8] F. Filippetti, G. Franceschini, C. Tassoni, P. Vas, Recent developments of induction motor drives fault diagnosis using AI techniques, IEEE Transactions on Industrial Electronics 47 (5) (2000) 994–1004.

[9] W.T. Thomson, M. Fenger, Current signature analysis to detect induction motor faults, IEEE Transactions on IAS Magazine 7 (4) (2001) 26–34.

[10] G.B. Kliman, J. Stein, Induction motor fault detection via passive current monitoring, International Conference on Electrical Machines 1 (1990) 13–17.

[11] R. Fiser, S. Ferkolj, Detecting side-band frequency components in stator current spectrum on induction motor for diagnosis purpose, Automatika, Journal for Control, Measurement, Electronics, Computing and Communications 40 (3–4) (1999) 155–160.

[12] G. Didier, H. Razik, A. Rezzoug, On the modelling of induction motor including the first space Harmonics for diagnosis purposes, International Conference on Electrical Machine, CD-Rom, Brugge, Belgium, August 2002.

[13] G. Didier, H. Razik, O. Caspary, E. Ternisien, Rotor cage fault detection in induction motor using global modulation index on the instantaneous power spectrum, Symposium on Diagnostics, Electric Machines, Power Electronics and Drives, CD-Rom, Atlanta, USA, August 2003.

[14] F. Filipetti, G. Franceschini, C. Tassoni, P. Vas, Impact of speed ripple on rotor fault diagnosis of induction machine, International Conference on Electrical Machines, Vigo, Spain, vol. 2, 1996, pp. 452–457.

[15] A.D. Poularikas, The Transforms and Applications Handbook, second ed., CRC Press, Boca Raton, FL.